SUPPLEMENTARY INFORMATION

Photogating-driven enhanced responsivity in few-layered $ReSe_2$ phototransistor

Received 00th January 20xx,
Accepted 00th January 20xx

DOI: 10.1039/x0xx00000x

Prasanna D. Patil,[a] Milinda Wasala,[a†] Rana Alkhaldi,[a] Lincoln Weber,[a] Kiran Kumar Kovi,[b] Bhaswar Chakrabarti,[b,c] Jawnaye A. Nash,[d] Daniel Rhodes,[e] Daniel Rosenmann,[b] Ralu Divan,[b] Anirudha V. Sumant,[b] Luis Balicas,[e] Nihar R. Pradhan[b,d,e,*] and Saikat Talapatra[a,*]

Estimation of contact resistance: y-function method

Ghibaudo proposed Y-function method[1], later modified by Chang *et. al.*[2], to estimate low-field mobility (μ_0) and effective contact resistance (R_C). Y-function is defined as $I_d/\sqrt{g_m}$ where I_d is drain current and g_m is transconductance, $\partial I_d/\partial V_g$. A detailed derivation can be found elsewhere.[2] For low-field bias condition ($V_g >> 0.5V_d$), drain current (I_d) and Y-function are given by Equation S1.1 and S1.2 respectively,

$$I_d = \left(\frac{\mu_0}{1+\theta\left(V_g - V_{th}\right)}\right) C_{ox}\, V_d\, \frac{W}{L}\left(V_g - V_{th}\right) \tag{S1.1}$$

$$Y = \frac{I_d}{\sqrt{g_m}} = \sqrt{\mu_0\, C_{ox}\, V_d\, \frac{W}{L}\left(V_g - V_{th}\right)} \tag{S1.2}$$

where all the symbol carry their meaning from main text and θ is effective attenuation factor, express as $\theta = \theta_0 + \mu_0.R_C.C_{ox}.W/L$ with θ_0 as first-order mobility attenuation coefficient.

Figure S1 shows Y-function analysis of device shown in main manuscript. Figure S1a shows plot of Y-function as function of gate voltage (V_g). Strong inversion region (V_g > 13 V), shown by cyan background, indicated a region where contact resistance (R_C) will be independent of applied gate voltage (V_g). From linear fit according to Equation S1.2 (red dotted line in Figure S1a), threshold voltage, V_{th} ~ 0.5 V and low-field mobility, μ_0 ~ 1.4 cm^2 V^{-1} s^{-1} were estimated from intercept and slope of linear fit, respectively. This value of low-field mobility of the same order as field-effect mobility (μ_{FE} ~ 4.6 cm^2 V^{-1} s^{-1}), indicating effect of contact resistance is minimal.[2]

Effective attenuation factor (θ) as a function of gate voltage (V_g), as shown in Figure S1b. In the limit of negligible θ_0, maximum contact resistance ($R_{C/max}$) can be estimated from $\theta \approx \mu_0.R_{C/max}.C_{ox}.W/L$. Maximum contact resistance ($R_{C/max}$) as well as total resistance of FET, $R_{tot} = V_d/I_d$, is shown in Figure S1c. At room temperature, maximum contact resistance is estimated to be $R_{C/max}$ ~ 773 kΩ and it is significantly lower than minimum channel resistance (R_{tot} ~ 2.4 MΩ) at V_g = 30 V. At lower V_g's, channel resistance (R_{tot}) increases whereas maximum contact resistance remains constant, as seen in Figure S1c. Temperature dependent $R_{C/max}$ and minimum R_{tot} are shown in Figure S1d. For all temperatures, $R_{C/max}$ is significantly lower than minimum R_{tot} thus we can conclude that contact resistance plays minimal role in conduction. Increase in contact resistance with decrease in temperature is a common signature of thermionic emission at metal-semiconductor junction.[3] The thermionic emission process supports the conduction mechanism in the semiconductor at room temperature where free electrons can easily tunnel through the barriers between semiconductor and metal junction to conduct. According to thermionic emission, contact resistance (R_C) as a function can be written as Equation S1.3,

$$R_C = R_0\, e^{\Phi_{SB}/k_B T} \tag{S1.3}$$

Upon fitting $\ln R_{C/max}$ with $1/k_BT$ (inset of Figure S1d), Schottky barrier height (Φ_{SB}) was estimated to be 117 meV.

In order to determine validity of contact resistance determined by Y-function method, we measured another device where contact resistance can be estimated by 4-probe method. Figure S2a and S2b shows transfer characteristics curves with 2-probe and 4-probe respectively. Contact resistance can be extract as difference between 2-probe resistance and 4-probe resistance, as shown in Figure S2c. Y-

[a] Department of Physics, Southern Illinois University Carbondale IL-62901, USA. Email: saikat@siu.edu.
[b] Center for Nanoscale Materials, Argonne National Laboratory, Argonne, IL-60439, USA.
[c] Institute for Molecular Engineering, University of Chicago, IL- 60637, USA.
[d] Department of Chemistry, Physics and Atmospheric Science, Jackson State University, Jackson, MS-39217, USA. Email: nihar.r.pradhan@jsums.edu.
[e] National High Magnetic Field Laboratory, Tallahassee, FL-32310, USA.
† Present Address: Science Department, Great Basin College, Elko, NV 89801, USA.
This is an Electronic Supplementary Information (ESI). For main manuscript, please see DOI: 10.1039/x0xx00000x

function analysis is performed on 2-probe transfer characteristics curve and it is shown in Figure S2d and S2e. Figure S2f shows contact resistance extracted from 2/4-probe method and maximum contact resistance estimated from Y-function method. As expected, both method shows similar contact resistances and Y-function overestimates contact resistance. Thus, contact resistance estimated by Y-function are reliable.

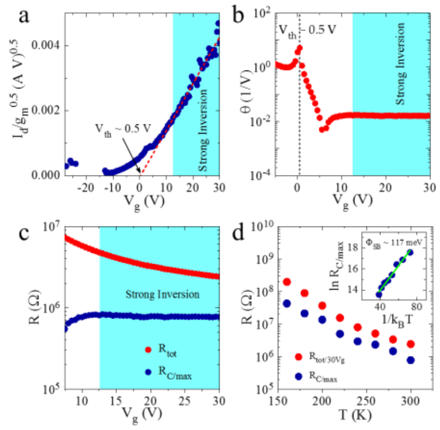

Figure S1. Y-function analysis of device presented in main manuscript. a) Y-function ($I_d/\sqrt{g_m}$) as a function of applied gate voltage (V_g). b) Effective attenuation factor (θ) as a function of V_g. c) Comparison of upper limit of contact resistance and total resistance of device (channel plus contact) in strong inversion region. d) Comparison of upper limit of contact resistance and lowest total resistance of device at V_g = 30 V as a function of temperature. Inset shows contact resistance in log scale as a function of $1/k_BT$ with linear fit (green line) used to estimate Schottky barrier height (Φ_{SB}).

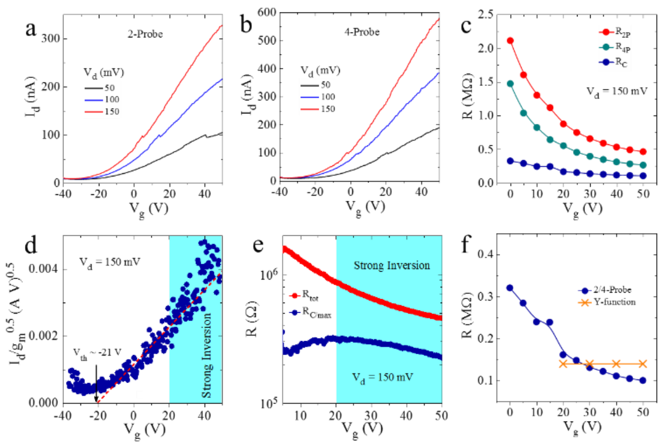

Figure S2. A comparison of contact resistance values estimated from different methods, two-/four-probe measurements (a-c) and Y-function method (d-e). a) Two-probe transfer characteristics (I_d *vs* V_g) for different drain voltages (V_d). b) Four-probe transfer characteristics (I_d *vs* V_g) for different drain voltages (V_d). c) Resistances for two- and four-probe and estimated contact resistance (R_C) as a function of V_g. d) Y-function ($I_d/\sqrt{g_m}$) as a function of applied gate voltage (V_g). e) A comparison of upper limit of contact resistance and total resistance of device (channel plus contact) in strong inversion region. f) A comparison of contact resistance estimated from two-/four-probe measurments and Y-function method.

External quantum efficiency (EQE)

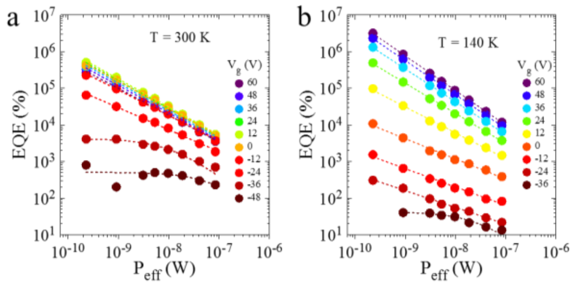

Figure S3. External quantum efficiency (EQE). a) EQE as a function of effective laser intensity (P_{eff}) under different applied gate voltages (-48 V < V_g < 60 V) at T = 300 K. b) EQE as a function of effective laser intensity (P_{eff}) under different applied gate voltages (-36 V < V_g < 60 V) at T = 140 K.

External quantum efficiency (EQE) determined photon conversion efficiency of photodetector and it is defined as ration of number of charge carrier in photocurrent to the total number of photon incident. EQE can be calculated by EQE = R×(h×c/e×λ) where R is responsivity, h is plank's constant, c is the speed of light, e is charge of electron and λ (= 640 nm) wavelength of the illuminated light. Figure S3 shows EQE as function of effective laser illumination intensity (P_{eff}) at temperature T = 300 K and 140 K (a and b respectively). Maximum EQE of ~ 10^6-10^7 % can be seen for lower illumination intensity. EQE of > 100 % suggests multiple photo carrier can be generates per incident photon. Possible origin for EQE of > 100 % could be attributed to either energy of incident photon (1.94 eV) higher than band gap of $ReSe_2$ (1.27 eV) or presence of photo-gain mechanisms such as photogating.[4, 5]

Output characteristics of device 2

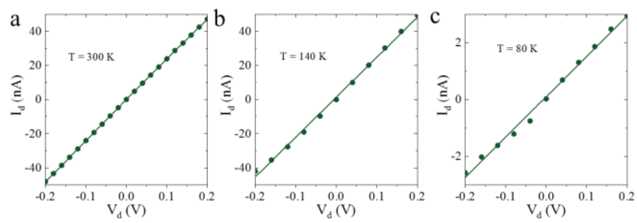

Figure S4. Output characteristics (I_d *vs* V_d) of device 2 at a) 300 K, b) 140 K and c) 80 K.

Output characteristics of device 2 at low temperatures (80 K < T < 300 K) are shown in Figure S4. Linear nature of the output characteristics curves, even at low temperatures, could be reasoned to the channel dominated conduction through the device and effect of contact resistance is minimal.

Electronic & optoelectronic transport of device 2

Further, we have measured another identical device and it is shown in Figure S5. Our investigations shows similar properties as device presented in main manuscript. We found field-effect mobility of μ_{FE} ~ 3.1 cm^2 V^{-1} s^{-1}, on/off ratio ~ 10^3 and subthreshold-swing of SS ~ 5.3 V/dec. Evidence of photogating (shift in threshold voltage V_{th} [Figure S5c] and decrease in Power exponent, γ, [Figure S5e]) can be clearly seen. Maximum responsivity R ~ 919 A W^{-1} can be found at effective laser intensity, P_{eff} ≈ 0.1 nW and gate voltage, V_g = 5 V

Figure S6 shows electronic & optoelectronic transport of device 2 at temperature T = 20 K. We found the field-effect mobility of μ_{FE} ~ 0.052 cm^2 V^{-1} s^{-1} with on/off ratio ~ 10^2. The channel current decreases at T = 20 K (Figure S6), which is a typical semiconductor characteristic. Maximum responsivity R ~ 430 A W^{-1} can be found at effective laser intensity, P_{eff} ≈ 0.1 nW and gate voltage, V_g = 30 V.

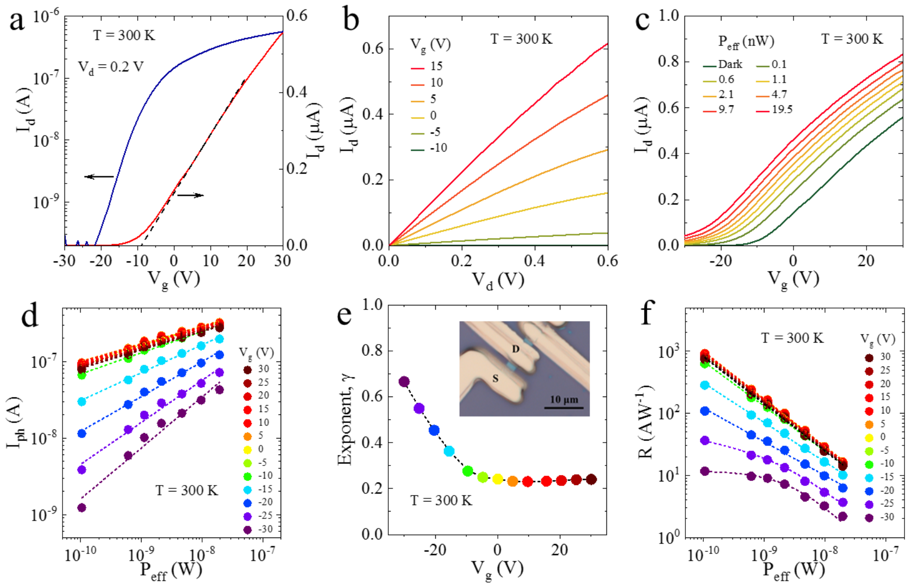

Figure S5. Electronic and optoelectronic transport of device 2 at T = 300 K. a) Transfer characteristics (I_d *vs* V_g) at V_d = 0.2V, in linear scale (red) and semi-log scale (blue). Black line indicates a region of curve utilized to calculate the field-effect mobility (μ_{FE}). b) Output characteristics (I_d *vs* V_d) under different applied gate voltages (-10 V < V_g < 15 V). c) Transfer characteristics (I_d *vs* V_g) at V_d = 0.2 V under laser illumination (λ = 640 nm) with different effective laser intensities (0.1 nW < P_{eff} < 19.5 nW). b) Photocurrent (I_{ph}) as a function of effective laser intensity (P_{eff}) under different applied gate voltages (-30 V < V_g < 30 V). Straight dashed line represents the fitting of $I_{ph} \propto (P_{eff})^{\gamma}$. c) Variation of power exponent (γ) as a function of applied gate voltage (V_g). d) Responsivity (R) as a function of effective laser intensity (P_{eff}) under different applied gate voltages (-30 V < V_g < 30 V). Dashed line indicates fitting of either $R \propto (P_{eff})^{(\gamma-1)}$ [6] or $R = A_1/(A_2 + P_{eff})$ [7].

Please do not adjust margins

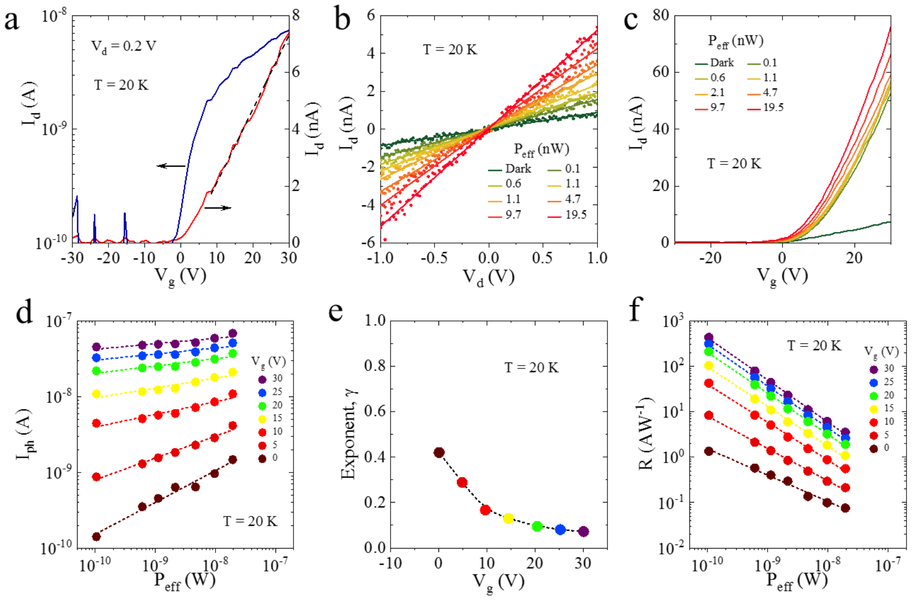

Figure S6. Electronic and optoelectronic transport of device 2 at T = 20 K. a) Transfer characteristics (I_d *vs* V_g) at V_d = 0.2V, in linear scale (red) and semi-log scale (blue). Black line indicates a region of curve utilized to calculate the field-effect mobility (μ_{FE}). b) Output characteristics (I_d *vs* V_d) under dark conditions and under different effective laser intensities (0.1 nW < P_{eff} < 19.5 nW). c) Transfer characteristics (I_d *vs* V_g) at V_d = 0.2 V under laser illumination (λ = 640 nm) with different effective laser intensities (0.1 nW < P_{eff} < 19.5 nW). b) Photocurrent (I_{ph}) as a function of effective laser intensity (P_{eff}) under different applied gate voltages (0 V < V_g < 30 V). Straight dashed line represents the fitting of $I_{ph} \propto (P_{eff})^{\gamma}$. c) Variation of power exponent (γ) as a function of applied gate voltage (V_g). d) Responsivity (R) as a function of effective laser intensity (P_{eff}) under different applied gate voltages (0 V < V_g < 30 V). Dashed line indicates fitting of $R \propto (P_{eff})^{(\gamma-1)}$ [6].

Notes and references

1. G. Ghibaudo, *Electronics Letters*, 1988, **24**, 543-545.
2. H.-Y. Chang, W. Zhu and D. Akinwande, *Applied Physics Letters*, 2014, **104**, 113504.
3. A. Pérez-Tomás, M. Placidi, A. Fontserè, P. M. Gammon and M. R. Jennings, *Microelectronics Reliability*, 2011, **51**, 1325-1329.
4. J. O. Island, S. I. Blanter, M. Buscema, H. S. J. van der Zant and A. Castellanos-Gomez, *Nano Letters*, 2015, **15**, 7853-7858.
5. S. Ghosh, P. D. Patil, M. Wasala, S. Lei, A. Nolander, P. Sivakumar, R. Vajtai, P. Ajayan and S. Talapatra, *2D Materials*, 2017, **5**, 015001.
6. H. Fang and W. Hu, *Advanced Science*, 2017, **4**, 1700323.
7. K. Roy, M. Padmanabhan, S. Goswami, T. P. Sai, G. Ramalingam, S. Raghavan and A. Ghosh, *Nature Nanotechnology*, 2013, **8**, 826-830.

